Electronic Supplementary Material (ESI) for Journal of Materials Chemistry C.

Supporting information for

Blue versus Yellow Emission in Bipolar Fluorenone Derivatives: Impact of Aggregation and Hydrogen Bonding

Nadzeya A. Kukhta[a, b], Dmytro Volyniuk[a], Juozas V. Grazulevicius* [a ,1] , Gjergji Sini*[c, 1]

[a]*Department of Organic Technology, Kaunas University of Technology, Radvilenu pl. 19, LT-50254, Kaunas, Lithuania*

[b] *Department of Chemistry, Durham University, South Road, Durham DH1 3LE, United Kingdom*

[c] *Laboratoire de Physicochimie des Polymères et des Interfaces, EA 2528 Université de Cergy-Pontoise, 5 mail Gay-Lussac, Cergy-Pontoise Cedex, 95031, France*

Supporting information

Contents

---

[1] Corresponding authors. Tel.: +370 37 300193; fax: +370 37 300152.
E-mail address: juozas.grazulevicius@ktu.lt, gjergji.sini@u-cergy.fr

I. Experimental details

I.1. Instrumentation

NMR spectra were recorded on Bruker DRX 500P spectrometer, and chemical shifts are reported in parts per million relative to solvent residue peek as an internal standard. ATR-FT-IR spectra were recorded on Bruker Vertex 70. Mass spectra were obtained by the MALDI-TOF method on Schimadzu Biothech Axima mass spectrometer. Elemental analysis data were obtained on a EuroEA Elemental Analyser. UV/Vis spectra of 10^{-4} M solutions of the compounds were recorded in quartz cells using Perkin Elmer Lambda 35 spectrometer. Photoluminescence (PL) spectra of 10^{-5} M solutions of the compounds were recorded using Edinburgh Instruments' FLS980 Fluorescence Spectrometer. Thin solid films for recording of UV/VIS and PL spectra were prepared by drop casting 2 mg/ml solutions of the compounds in toluene on the pre-cleaned quartz substrates. Solid solutions of the molecularly dispersed compounds in polystyrene and zeonex polymer matrices were obtained with the concentrations of 0.25 wt% and 1 wt%, respectively, were prepared by mixing the dissolved compounds and polymer in toluene solutions at appropriate ratio and casting the solutions on quartz substrates in an ambient air. Fluorescence quantum yields (η) of the solutions and of the solid films were estimated using the integrated sphere method [1]. Emission was focused onto a spectrograph and detected on a sensitive gated iCCD camera (Stanford Computer Optics) having sub-nanosecond resolution. A model liquid nitrogen cryostat (Janis Research) was used for the experiment. The highest energy peak in the phosphorescence spectrum was taken for the $T^1 \rightarrow S^0$ transition [2].

Thermogravimetric analysis (TGA) was performed on a Metter TGA/SDTA851e/LF/1100 apparatus at a heating rate of 20 ^{o}C/min under nitrogen atmosphere. Differential scanning calorimetry (DSC) measurements were done on a DSC Q 100 TA Instrument at a heating rate of 10^{o}C/min under nitrogen atmosphere. Cyclic voltammetry (CV) measurements were carried out with a glassy carbon working electrode in a three electrode cell. The measurements were performed using Eco Chemie Company's AUTOLAB potentiostat "PGSTAT20" in the dry dichloromethane solution containing 0.1 M tetrabutylammonium hexafluorophosphate ($TBAPF_6$) as the electrolyte at room temperature under nitrogen atmosphere. The results were collected using GPES (General Purpose Electrochemical System) software. The electrochemical cell comprised platinum wire with 1 mm diameter of working area as working electrode, Ag wire e calibrated versus ferrocene/ferrocinium redox couple e as a quasi-reference electrode and platinum coil as auxiliary electrode. Cyclovoltammperometric measurements were conducted at 50 mV/s potential rate.

The ionization potentials (IP) of the layers of the synthesized compounds were measured by the electron photoemission method in air [2]. The experiment setup of this method was similar to previously described one [3]. We recorded the electron photoemission spectra for the solid state layers of studied compounds which were casted from the solutions in tetrahydrofuran (THF) onto pre-cleaned indium tin oxide (ITO) coated glass substrates. Using the deep UV deuterium light source ASBN-D130-CM and CM110 1/8m monochromator, the layers were illuminated by the monochromatic light ranging from 350 nm to 190 nm with step of 2 nm. A 6517B Keithley electrometer was utilized for applying electric field to the layers and measuring the photocurrent (i) which was flowing in the circuit under illumination with photon energy higher than IP_{EP} of studied compounds.

Charge drift mobility measurements were performed by a time-of-flight (TOF) method. The samples for the TOF measurements were prepared by spin-coating of the solutions of the synthesized compounds in toluene on the pre-cleaned ITO coated glass plates with the thickness of a layer 0.7, 5 and 0.75 μm for **FN-TPA**, **FN-TPB** and **FN-PCz**, respectively. A top aluminum electrode of 60 nm thick was deposited by thermal evaporation under vacuum below 5×10^{-6} mbar, while the sample area was of 6 mm^2 with 7 samples per substrate. The light pulse was used to photo generate the charge carriers by exciting layers of compounds through the ITO electrode. The positive voltage was applied to the ITO electrode for hole mobility measurements, otherwise the negative voltage was applied to the ITO electrode for electron mobility measurements. Charges were generated by a pulsed third-harmonic Nd:YAG laser EKSPLA NL300 working at a pulse duration of 3-6 ns and the wavelength of 355 nm. Electric fields were applied by a Keithley 6517B electrometer. A digital storage oscilloscope Tektronix TDS 3032C was used to record ToF transients. The transit time t_{tr} for the samples with the charge transporting material was determined by the kink on the curve of the transient in log–log scale (Figure S4). The drift mobility was calculated using the formula $\mu=d^2/Ut_{tr}$, where d is the layer thickness, and U is the surface potential at the moment of illumination.

I.2. Computational Methods

Different density functional theory (DFT) [4] methods were employed for the calculations in this study using the Gaussian 09 quantum chemical package [5]. Full geometry optimizations of the compounds in their electronic ground state were performed with DFT using the B3LYP [6] functional with the 6-31G basis set in vacuum. The energies of the highest occupied (HOMO) and the lowest unoccupied (LUMO) molecular orbitals were obtained from single point calculations in the framework of DFT BMK/6-31G approach in gas phase. The theoretical absorption spectra were simulated from the oscillator strengths of singlet transitions calculated by the TD-DFT BMK/6-31G method in vacuum.

Various DFT methods were employed in order to (i) consider the ensemble of orbital-to-orbital transitions contribution to a given excited state and (ii) to make use of functionals taking into account the correct contribution of the charge transfer transitions. The first requirement can be satisfied by calculation the natural transition orbitals (NTO) [7], whereas the second one can be satisfied by considering functionals containing high percentage of Hartree-Fock (%HF) contribution to the calculation of the exchange energy [8].

I.3. Materials

The starting compounds i.e. 9*H*-carbazole, triphenylamine, fluorenone, 1-(4-iodophenyl)ethanone, 1-bromo-4-iodobenzene, and the required chemicals, i.e. 2-chloro-2-methylpropane, ethynyltrimethylsilane, triphenylphosphine (PPh_3), *bis*-triphenylphosphine palladium(II) dichloride ($Pd(PPh_3)_2Cl_2$), copper iodide (CuI), tetra-*n*-butylammonium fluoride (*n*-Bu_4NF) solution in THF, copper (Cu), 18-crown-6, potassium iodide (KI), potassium iodate (KIO_3), potassium carbonate (K_2CO_3), anhydrous sodium sulfate (Na_2SO_4), silicon tetrachloride ($SiCl_4$), aluminum trichloride ($AlCl_3$), *N*-bromosuccinimide (NBS), *N*-iodosuccinimide (NIS) were purchased from Sigma-Aldrich and used as received. Zeonex cyclo-olefin polymer was purchased from ZEON Corporation. The solvents, i.e. chloroform, *n*-hexane,dichloromethane, ethanol, tetrahydrofurane (THF), acetic acid (AcOH), dichloromethane (Poch), *N,N*-dimethylformamide (DMF) and *N, N*-diisopropylamine (*i*-PrA) (Sigma-Aldrich) were dried and distilled according the conventional procedures [9].

4-Bromo-*N,N*-bis(4-iodophenyl)aniline (**1**) and 9-(4-bromophenyl)-3,6-diiodo-9*H*-carbazole (**3**) were obtained by the reported procedures [10–12].1,3,5-Tris(4-iodophenyl)benzene (**2**) was prepared by the electrophilic cyclization according to the known procedure [13].The usage of Friedel-Crafts alkylation as described in literature source [14] yielded 3,6-di-*tert*-butylcarbazole **(4)**.2,7-Diiodo-9*H*-fluoren-9-one (**5**) was synthesized by the reported method [15].

I.4 Synthesis and characterization of the intermediate and target compounds

Method A: general procedure for Ulmann condensation. In the two-neck round-bottom arylhalide (1 molar eq.), arylamine (1.5 molar eq.) and 18-crown-6 (0.2 molar eq.) were dissolved in DMF (15 mL) under argon atmosphere. After the reaction mixture was heated up to 100 ^{o}C, potassium carbonate K_2CO_3 (6 molar eq.) was added, which was followed by the addition of copper Cu (3 molar eq.). The reaction mixture was stirred for 24 h at 140 ^{o}C. After being cooled down to room temperature, the reaction mixture was filtered and carefully washed with chloroform. The solvents were evaporated under reduced pressure, and the crude material was purified by the column chromatography on silica gel using hexane: toluene 10:1 as eluent and precipitation to methanol.

Method B: general procedure for Sonogashira-Hagihara cross-coupling reaction [16]. Substituted acetylene (1.5 molar eq.) was added to the mixture of arylhalide (1 molar eq.), $Pd(PPh_3)_2Cl_2$ (0.02 molar eq.), CuI (0.012 molar eq.) and PPh_3 (0.1 molar eq.) in the mixture of dry *i*-PrA (10 mL) and THF (10 mL) under the argon atmosphere. After being stirred for 24 h at 90˚C the reaction mixture was treated with water, extracted with chloroform and washed with brine twice. The organic phase was dried over anhydrous Na_2SO_4. After evaporation of the solvent under reduced pressure the residue was purified by silica gel chromatography using hexane: toluene 10:1 as an eluent and precipitation to methanol. In the case of final coupling the amount of the substituted acetylene and catalysts should be doubled.

Method C: general procedure for the trimethylsilyl group cleavage [17]. 2.5M Solution of *n*-Bu_4NF in THF (1.5 molar eq.) was added dropwise to the vigorously stirred solution of arylethynyltrimethylsilane (1 molar eq.) in anhydrous THF (10 mL) under argon atmosphere. After being stirred for 2 h at the room temperature the reaction mixture was treated with water, extracted with dichloromethane and washed with brine twice. The organic layer was dried over anhydrous Na_2SO_4. After evaporation of the solvent under reduced pressure the residue was precipitated to methanol.

4-Bromo-N,N-bis(4-(3,6-di-tert-butyl-9H-carbazol-9-yl)phenyl)aniline (1a) was prepared by method A. Off-white solid (2.00 g, yield 86%). ^{1}H NMR (300 MHz, $CDCl_3$, δ): 8.17 (d, 4H, *J* = 1.62 Hz), 7.50-7.53 (m, 10H), 7.43 (d, 4H, *J* = 8.58 Hz), 7.38 (d, 4H, *J* = 8.50 Hz), 7.21 (d, 2H, *J* =

8.68 Hz), 1.50 (s, 36H, CH_3-).^{13}C NMR (300 MHz, $CDCl_3$, δ): 145.8, 142.8, 139.3, 133.2, 132.7, 127.7, 126.1, 125.1, 123.6, 123.3, 116.3, 109.2, 34.8 (C−CH_3), 32.0 (CH_3-).

9,9'-(5'-(4-Iodophenyl)-[1,1':3',1''-terphenyl]-4,4''-diyl)bis(3,6-di-tert-butyl-9H-carbazole) (2a) was prepared by method A. Off-white solid (1.57g, yield 63%). ^{1}H NMR (300 MHz, $CDCl_3$, δ): 8.09 (d, 4H, *J* = 1.69 Hz), 7.91 (t, 1H, *J* = 1.66 Hz), 7.86 (d, 4H, *J* = 8.32 Hz), 7.80 (d, 2H, *J* = 1.51 Hz), 7.78 (d, 2H, *J* = 8.38 Hz), 7.62 (d, 4H, *J* = 8.33 Hz), 7.45 (d, 2H, *J* = 8.41 Hz), 7.42 (dd, 4H, *J* = 8.57 Hz, *J* = 1.81 Hz), 7.37 (d, 4H, *J* = 8.58 Hz), 1.38 (s, 36H, CH_3-).^{13}C NMR (300 MHz, $CDCl_3$, δ): 143.1, 142.0, 141.5, 140.5, 139.3, 139.1, 138.1, 137.9, 129.2, 128.7, 127.1, 125.5, 125.0, 123.7, 123.5, 116.3, 109.3, 93.6 (C−I), 34.8 (C−CH_3), 32.0 (CH_3-).

9'-(4-Bromophenyl)-3,3'',6,6''-tetra-tert-butyl-9'H-9,3':6',9''-tercarbazole (3a) was prepared by method A. Off-white solid (1.80g, yield 78%). ^{1}H NMR (300 MHz, $CDCl_3$, δ): 8.16 (t, 2H, *J* = 1.29 Hz), 8.08 (d, 4H, *J* = 1.61 Hz), 7.76 (d, 2H, *J*=8.63 Hz), 7.55 (d, 3H, *J* = 8.63 Hz), 7.53 (d, 3H, *J* = 1.76 Hz), 7.38 (dd, 4H, *J* =8.67 Hz, *J* = 1.82 Hz), 7.24 (d, 4H, *J* = 8.63 Hz), 1.39 (s, 36H, CH_3-).^{13}C NMR (300 MHz, $CDCl_3$, δ): 142.6, 140.1, 133.6, 128.8, 124.1, 123.6, 123.2, 119.4, 116.2, 109.1, 34.7 (C−CH_3), 32.0 (CH_3-).

4-(3,6-Di-tert-butyl-9H-carbazol-9-yl)-N-(4-(3,6-di-tert-butyl-9H-carbazol-9-yl)phenyl)-N-(4-((trimethylsilyl)ethynyl)phenyl)aniline (1b) was prepared by method B. White solid (1.87 g, yield 92%).^{1}H NMR (300 MHz, $CDCl_3$, δ): 8.19 (d, 4H, *J* = 1.62 Hz), 7.49-7.52 (m, 10H), 7.43 (d, 4H, *J* = 8.58 Hz), 7.37 (d, 4H, *J* = 8.50 Hz), 7.20 (d, 2H, *J* = 8.68 Hz), 1.50 (s, 36H, CH_3-), 0.32 (s, 9H, Si−CH_3).^{13}C NMR (300 MHz, $CDCl_3$, δ): 145.8, 142.8, 139.3, 133.2, 132.7, 127.7, 126.1, 125.1, 123.6, 123.3, 116.3, 110.2, 104.0 (C≡C), 96.2 (C≡C), 34.7 (C−CH_3), 32.0 (CH_3-), 0 (Si−CH_3).

9,9'-(5'-(4-((Trimethylsilyl)ethynyl)phenyl)-[1,1':3',1''-terphenyl]-4,4''-diyl)bis(3,6-di-tert-butyl-9H-carbazole) (2b) was prepared by method B. White solid (1.38 g, yield 90 %).^{1}H NMR (300 MHz, $CDCl_3$, δ): 8.19 (d, 4H, *J* = 1.41 Hz), 8.01 (t, 1H, *J* = 1.54 Hz), 7.97 (d, 4H, *J* = 8.50 Hz), 7.94 (d, 2H, *J* = 1.62 Hz), 7.77 (d, 2H, *J* = 8.49 Hz), 7.73 (d, 4H, *J* = 8.50 Hz), 7.65 (d, 2H, *J* = 8.50 Hz), 7.52 (dd, 4H, *J* = 8.68 Hz, *J* = 1.87 Hz), 7.47 (d, 4H, *J* = 8.54 Hz), 1.51 (s, 36H, CH_3-), 0.32 (s, 9H, Si−CH_3).^{13}C NMR (300 MHz, $CDCl_3$, δ):143.0, 141.8, 140.8, 139.4, 139.1, 137.8, 132.6, 128.7, 127.1, 127.0, 125.2, 123.7, 123.5, 122.6, 116.3, 109.2, 104.8 (C≡C), 95.3 (C≡C), 34.7 (C−CH_3), 32.0 (CH_3-), 0 (Si−CH_3).

3,3'',6,6''-Tetra-tert-butyl-9'-(4-((trimethylsilyl)ethynyl)phenyl)-9'H-9,3':6',9''-tercarbazole (3b) was prepared by method B. White solid (1.52 g, yield 87 %).^{1}H NMR (300 MHz, $CDCl_3$, δ):

8.06-8.09 (m, 2H), 8.00 (d, 4H, J = 1.45 Hz), 7.64 (d, 2H, J = 8.28 Hz), 7.53 (d, 2H, J = 8.39 Hz), 7.47 (d, 2H, J = 8.61), 7.45 (dd, 2H, J = 8.66 Hz, J= 1.85 Hz), 7.30 (d, 4H, J = 8.58 Hz), 7.18 (d, 4H, J = 8.61 Hz), 1.30 (s, 36H, CH$_3$-), 0.16 (s, 9H, Si−CH$_3$). ^{13}C NMR (300 MHz, CDCl$_3$, δ): 142.6, 140.1, 137.2, 133.8, 131.2, 126.9, 126.1, 124.1, 123.6, 123.1, 119.3, 116.3, 111.2, 109.1, 104.0 (C≡C), 96.0 (C≡C), 34.9 (C−CH$_3$), 32.1 (CH$_3$-), 0 (Si−CH$_3$).

4-(3,6-Di-tert-butyl-9H-carbazol-9-yl)-N-(4-(3,6-di-tert-butyl-9H-carbazol-9-yl)phenyl)-N-(4-ethynylphenyl)aniline (1c) was prepared by method C. White solid (1.65 g, yield 96 %).^{1}H NMR (300 MHz, CDCl$_3$, δ): 8.17 (d, 4H, J = 1.57 Hz), 7.48-7.54 (m, 10H), 7.44 (d, 4H, J = 8.72 Hz), 7.41 (d, 4H, J = 8.76 Hz), 7.23 (d, 2H, J = 8.70 Hz), 3.77 (s, 1H, C≡C−H), 1.50 (s, 36H, CH$_3$-).^{13}C NMR (300 MHz, CDCl$_3$, δ): 145.6, 142.9, 139.3, 127.6, 125.6, 123.6, 123.4, 123.1, 116.2, 109.2, 84.3 (C≡C), 68.0 (C≡C), 34.8 (C−CH$_3$), 32.0 (CH$_3$-).

9,9'-(5'-(4-Ethynylphenyl)-[1,1':3',1''-terphenyl]-4,4''-diyl)bis(3,6-di-tert-butyl-9H-carbazole) (2c) was prepared by method C. Off-white solid (1.13 g, yield 89 %).^{1}H NMR (300 MHz, CDCl$_3$, δ): 8.10 (d, 4H, J = 1.34 Hz), 7.92-7.96 (m, 4H), 7.87 (d, 2H, J = 8.50 Hz), 7.84 (d, 1H, J = 1.52 Hz), 7.69 (d, 2H, J = 8.45 Hz), 7.61 (d, 4H, J = 8.48 Hz), 7.56 (d, 2H, J = 8.26 Hz), 7.40 (dd, 4H, J = 8.72 Hz, J = 1.84 Hz), 7.38 (d, 4H, J = 8.67 Hz), 3.72 (s, 1H, C≡C−H), 1.62 (s, 36H, CH$_3$-).^{13}C NMR (300 MHz, CDCl$_3$, δ): 142.6, 141.3, 141.2, 140.8, 138.6, 137.4, 132.3, 128.2, 126.8, 126.4, 124.9, 124.6, 123.4, 122.9, 115.9, 108.9, 82.9 (C≡C), 68.4 (C≡C), 34.3 (C−CH$_3$), 31.6 (CH$_3$-).

3,3'',6,6''-Tetra-tert-butyl-9'-(4-ethynylphenyl)-9'H-9,3':6',9''-tercarbazole (3c) was prepared by method C. Off-white solid (1.34 g, yield 92 %).^{1}H NMR (300 MHz, CDCl$_3$, δ): 8.16 (d, 2H, J = 1.78 Hz), 8.08 (d, 4H, J = 1.67 Hz), 7.75 (d, 2H, J = 8.45 Hz), 7.65 (d, 2H, J = 8.47 Hz), 7.57 (d, 2H, J = 8.61 Hz), 7.53 (dd, 2H, J = 8.65 Hz, J = 1.98 Hz), 7.38 (dd, 4H, J = 8.43 Hz, J = 1.91 Hz), 7.25 (d, 4H, J = 8.72 Hz), 3.16 (s, 1H, C≡C−H), 1.39 (36H, , CH$_3$-).^{13}C NMR (300 MHz, CDCl$_3$, δ): 142.6, 140.1, 139.9, 137.6, 134.0, 131.2, 126.9, 126.1, 124.2, 123.6, 123.1, 121.8, 119.3, 116.2, 111.1, 109.1, 82.7 (C≡C), 78.6 (C≡C), 34.7 (C−CH$_3$), 32.1 (CH$_3$-).

*2,7-Bis((4-(bis(4-(3,6-di-tert-butyl-9H-carbazol-9-yl)phenyl)amino)phenyl)ethynyl)-9H-fluoren-9-one (**FN-TPA**)* was prepared by method B. Orange solid (1.16 g, yield 83 %). ^{1}H NMR (300 MHz, CDCl$_3$, δ): 8.07 (d, 8H, J = 1.60 Hz), 7.75 (d, 2H, J = 0.87 Hz), 7.58 (dd, 2H, J = 7.74 Hz, J = 1.22 Hz), 7.74-7.76 (m, 12H), 7.42 (dd, 8H, J = 8.62 Hz, J = 1.78 Hz), 7.35 (d, 8H, J = 8.62 Hz), 7.33 (d, 8H, J = 8.67 Hz), 7.18 (d, 6H, J = 8.59 Hz), 1.40 (s, 72H, CH$_3$-). ^{13}C NMR (300 MHz,

$CDCl_3$, δ): 192.4 (C=O), 147.8, 145.5, 143.1, 142.9, 139.3, 137.7, 134.5, 133.7, 133.0, 127.8, 127.4, 125.7, 124.7, 123.7, 123.3, 123.1, 120.5, 116.6, 116.3, 109.2, 91.7 (C≡C), 88.4 (C≡C), 34.7 (C−CH_3), 32.0 (CH_3-). ATR-FTIR (ν_{max}/cm^{-1}): 3022 (=C−H), 2962 (C−H), 2862, 2240 (C≡C), 1748 (C=O), 1603, 1498 (C=C Ar), 1366, 1302, 1267 (=C−N), 810 (C−H Ar). MALDI-TOF MS (m/z): calculated for $C_{133}H_{126}N_6O$ 1824.46 (M^++H), found 1824.76. Anal. calc. for $C_{133}H_{126}N_6O$: C 87.56; H 6.96; N 4.61; O 0.88; found: C; 87.55; H 6.93; N 4.63; O 0.89.

2,7-Bis((4''-(3,6-di-tert-butyl-9H-carbazol-9-yl)-5'-(4-(3,6-di-tert-butyl-9H-carbazol-9-yl)phenyl)-[1,1':3',1''-terphenyl]-4-yl)ethynyl)-9H-fluoren-9-one (**FN-TPB**) was prepared by method B. Yellow solid (0.73 g, yield 74 %). ^{1}H NMR (300 MHz, $CDCl_3$, δ): 8.09 (d, 8H, *J*= 1.62 Hz), 7.92 (t, 2H, *J* = 1.34 Hz), 7.88 (d, 12H, *J* = 8.26 Hz), 7.79 (d, 2H, *J* = 0.78 Hz), 7.73 (d, 4H, *J* = 8.23 Hz), 7.62-7.65 (m, 14H), 7.47 (d, 2H, *J* = 7.75 Hz), 7.42 (dd, 8H, *J* = 8.62 Hz, *J* = 1.84 Hz), 7.37 (d, 8H, *J* = 8.58 Hz), 1.41 (s, 72H, CH_3-). ^{13}C NMR (300 MHz, $CDCl_3$, δ): 192.2 (C=O), 143.3, 143.0, 141.9, 141.7, 141.1, 139.4, 139.2, 137.9, 137.8, 134.5, 132.3, 128.7, 127.5, 127.4, 127.1, 125.5, 125.2, 124.5, 123.7, 123.5, 122.2, 120.7, 116.3, 109.2, 91.4 (C≡C), 89.6 (C≡C), 34.7 (C−CH_3), 32.0 (CH_3-). ATR-FTIR (ν_{max}/cm^{-1}): 3026 (=C−H), 2967 (C−H), 2862, 2215 (C≡C), 1741 (C=O), 1599, 1465 (C−H Ar), 1366, 1302, 1218 (=C−N), 789 (C−H Ar). MALDI-TOF MS (m/z): calculated for $C_{145}H_{132}N_4O$ 1946.63 (M^++H), found 1945.19. Anal. calc. for $C_{145}H_{132}N_4O$: C 89.46; H 6.84; N 2.88; O 0.82; found: C; 89.45; H 6.87; N 2.87; O 0.81.

2,7-Bis((4-(3,3'',6,6''-tetra-tert-butyl-9'H-[9,3':6',9''-tercarbazol]-9'-yl)phenyl)ethynyl)-9H-fluoren-9-one (**FN-PCz**) was prepared by method B. Yellow solid (0.94 g, yield 79 %). ^{1}H NMR (300 MHz, $CDCl_3$, δ): 8.17 (d, 4H, *J* = 1.83 Hz), 8.09 (d, 8H, *J* = 1.64 Hz), 7.84 (d, 2H, *J* = 0.82 Hz), 7.79 (d, 4H, *J* = 8.27 Hz), 7.69 (d, 4H, *J* = 8.49 Hz), 7.67 (d, 2H, *J* = 1.24 Hz), 7.61 (d, 4H, *J* = 8.63 Hz), 7.55 (dd, 4H, *J* = 8.50 Hz, *J* = 1.95 Hz), 7.52 (d, 2H, *J* = 7.61 Hz), 7.38 (dd, 8H, *J* = 8.61 Hz, *J* = 1.83 Hz), 7.27 (d, 8H, *J* = 8.59 Hz), 1.39 (s, 72H, CH_3-). ^{13}C NMR (300 MHz, $CDCl_3$, δ): 192.2 (C=O), 143.5, 142.6, 140.1, 138.0, 137.5, 134.6, 133.5, 131.3, 129.1, 128.2, 127.6, 127.0, 126.1, 124.2, 123.6, 123.2, 122.4, 120.8, 119.4, 116.2, 111.1, 109.1, 90.6 (C≡C), 89.9 (C≡C), 34.7 (C−CH_3), 32.0 (CH_3-). ATR-FTIR (ν_{max}/cm^{-1}): 3021 (=C−H), 2966 (C−H), 2871, 2211 (C≡C), 1742 (C=O), 1549, 1494 (C−H Ar), 1368, 1303, 1218 (=C−N), 808 (C−H Ar). MALDI-TOF MS (m/z): calculated for $C_{133}H_{122}N_6O$ 1819.97 (M^++H), found 1819.02. Anal. calc. for $C_{133}H_{122}N_6O$: C 87.75; H 6.76; N 4.62; O 0.88; found: C; 88.03; H 6.78; N 4.29; O 0.90.

II. Figures

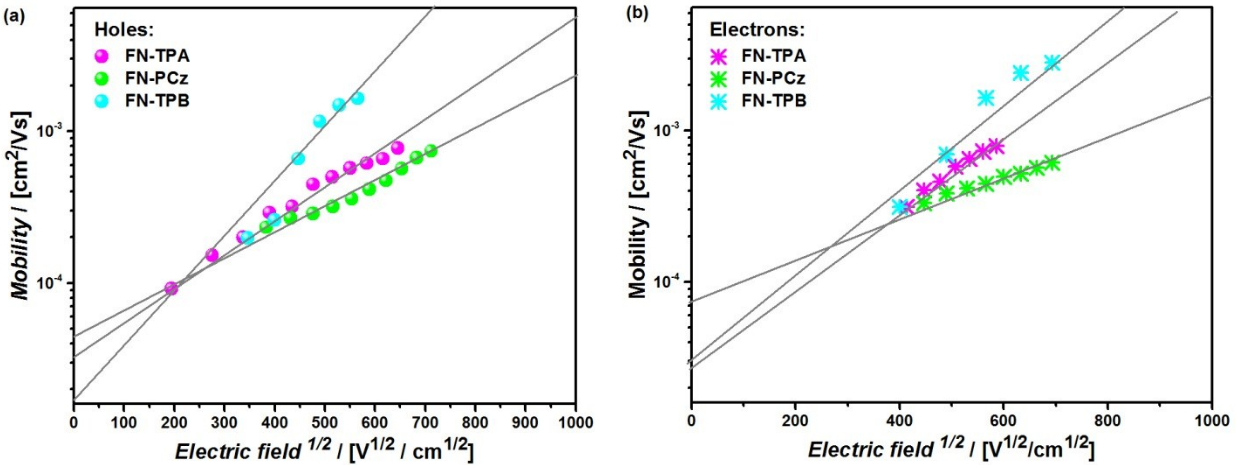

Figure S1. Electric field dependencies of (b) hole and (c) electron drift mobilities, measured by TOF method at room temperature, of **FN-TPA**, **FN-TPB** and **FN-PCz**.

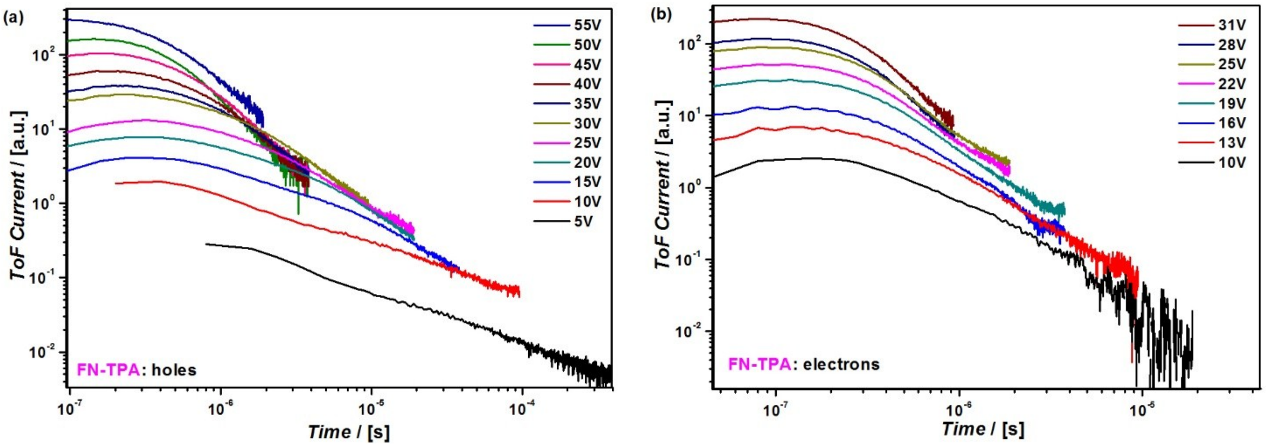

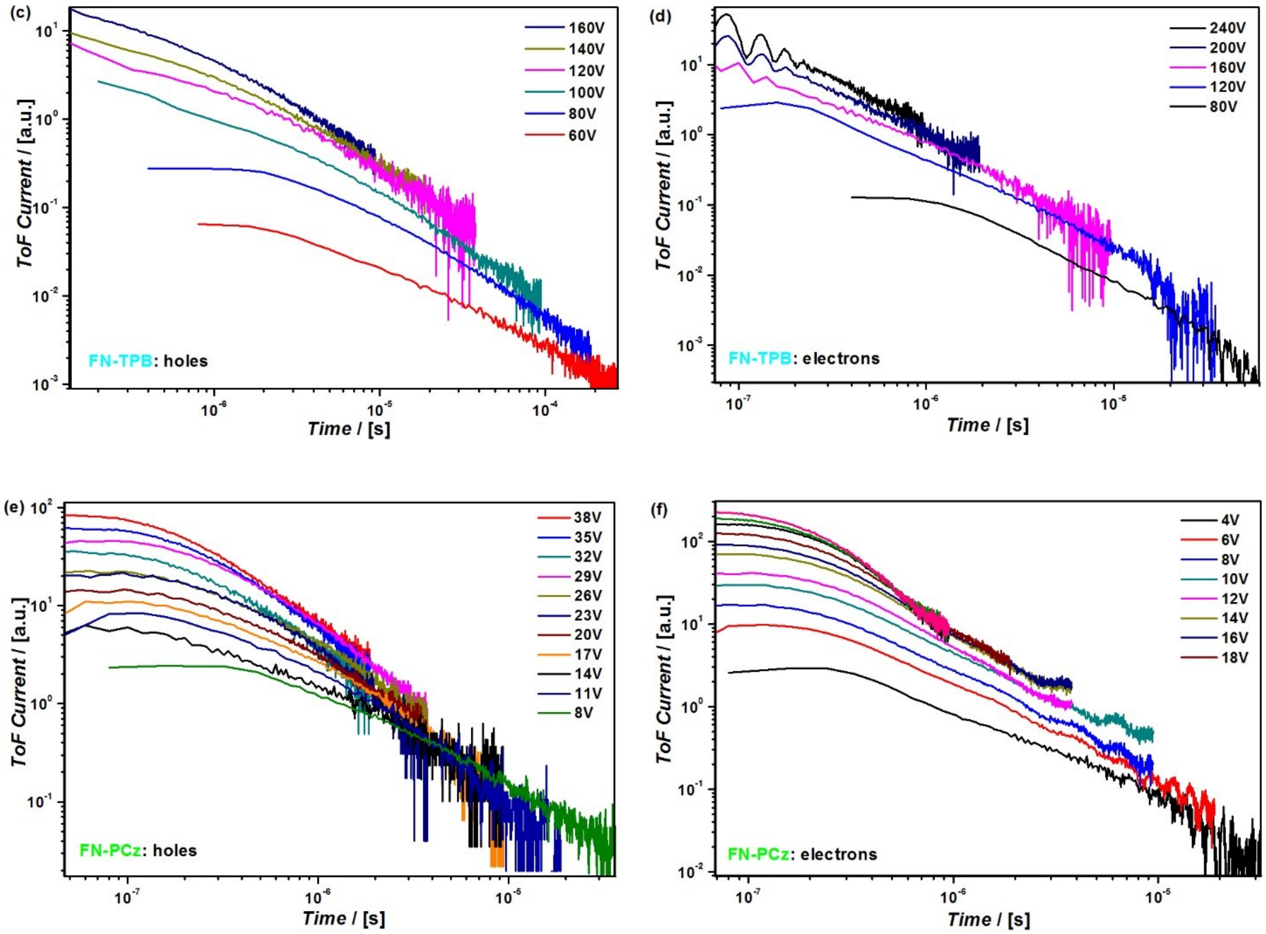

Figure S2. Current transient pulses at different electric fields and room temperature for **FN-TPA** (a) holes, (b) electrons; **FN-TPB** (c) holes, (d) electrons; **FN-PCz** (e) holes, (f) electrons.

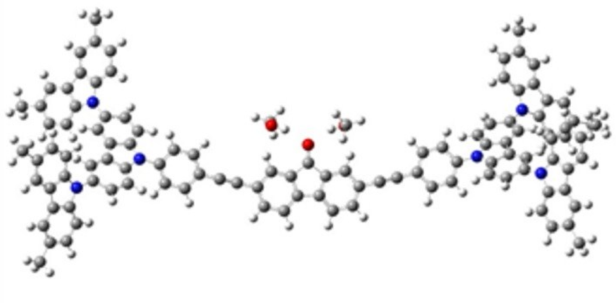

Figure S3. The optimized geometry of H-bonded complex **FN-PCz**, obtained at the ωB97XD/6-31G level in gas phase. Reproduced with permission from the editors. Copyright © 2017, American Chemical Society.

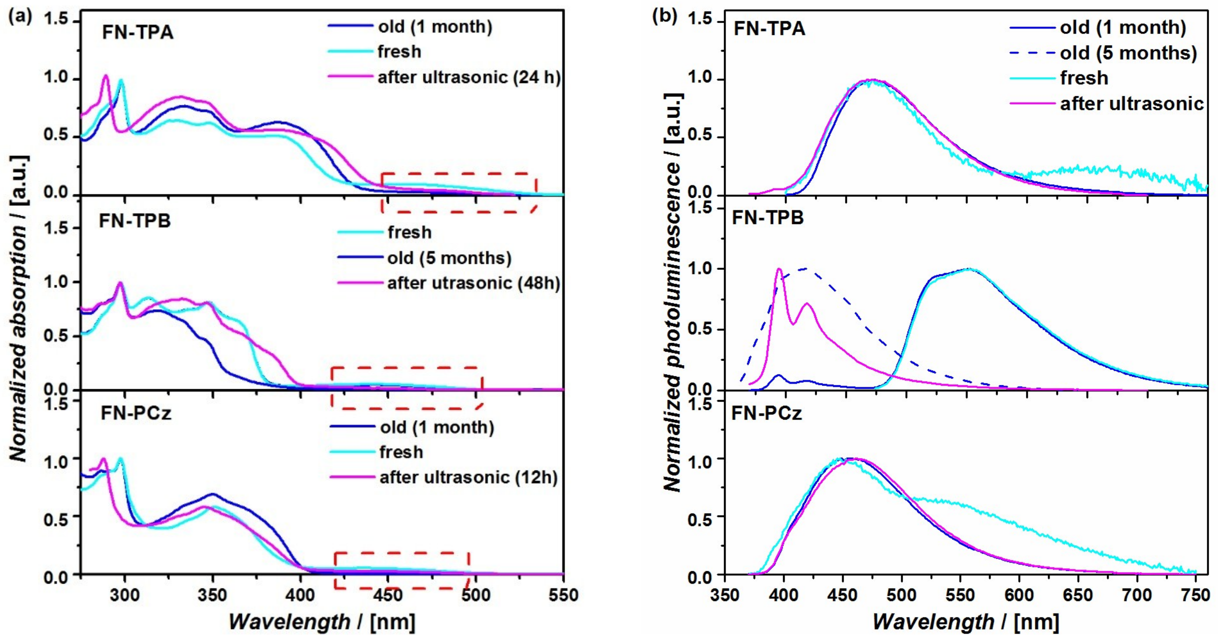

Figure S4. (a) Normalized absorption spectra and (b) PL spectra (λ_{ex} = 350 nm) of old, fresh and sonicated THF 10^{-5}M solutions of **FN-PCz**, **FN-TPB** and **FN-PCz**.

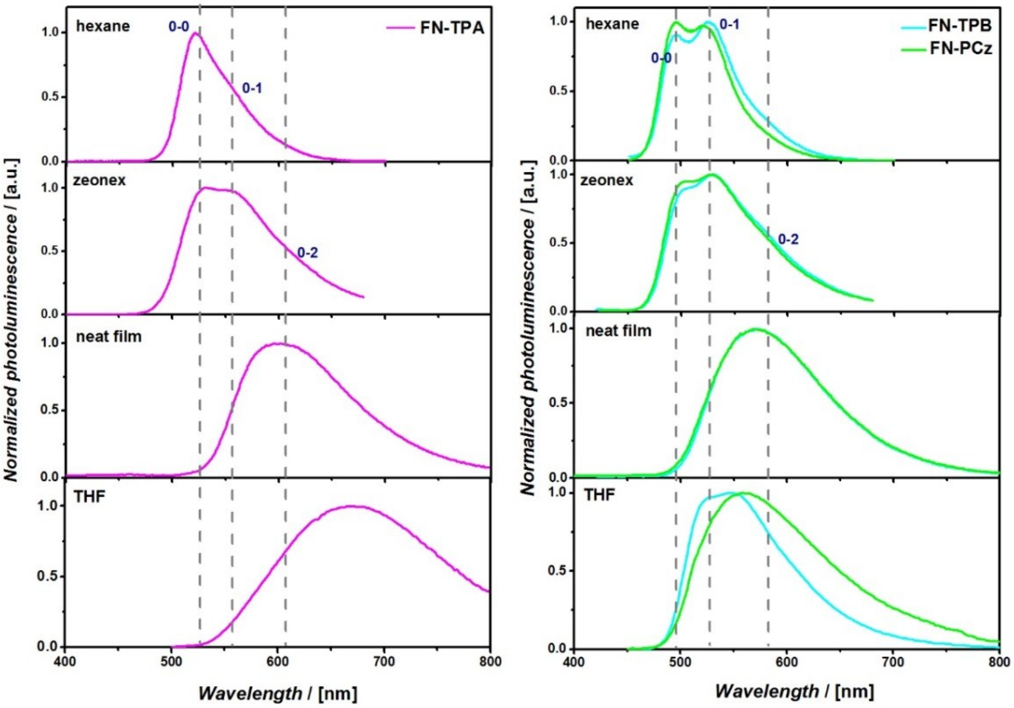

Figure S5. Comparison of the photoluminescence spectra of **FN-TPA**, **FN-TPB** and **FN-PCz**, recorded in different media.

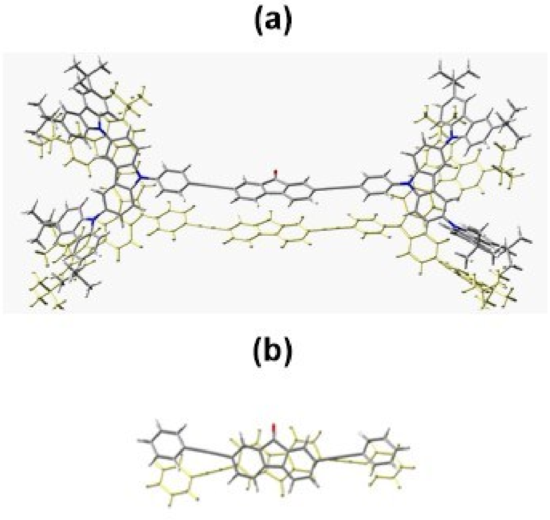

Figure S6. Structures of the model dimers for (a) **FN-PCz** (cofacial) and (b) **FN-di(CCPh)** (antiparallel), estimated at the wB97XD/6-31G level in gas phase. Reproduced with permission from the editors. Copyright © 2017, American Chemical Society.

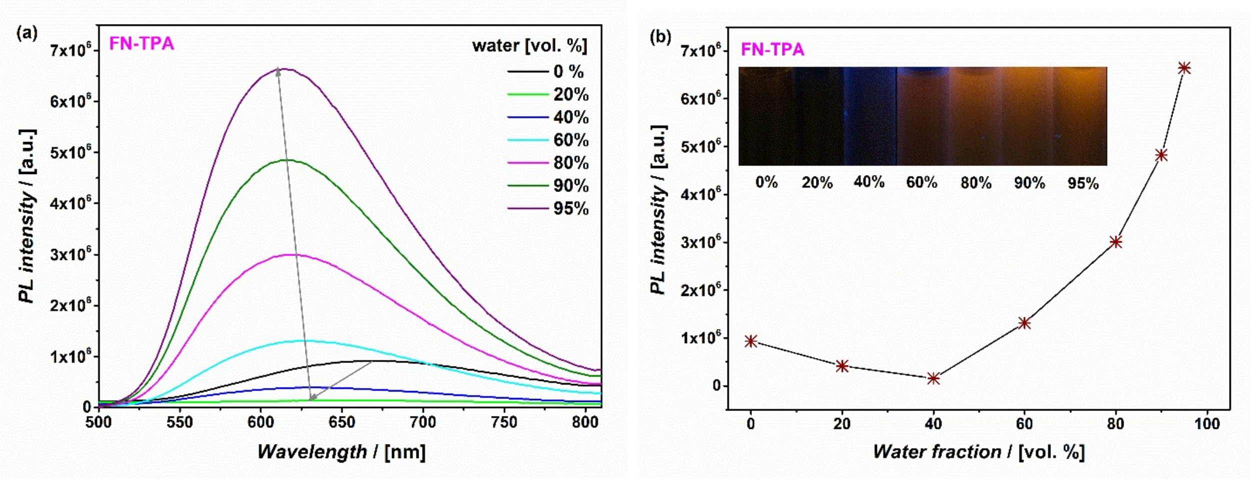

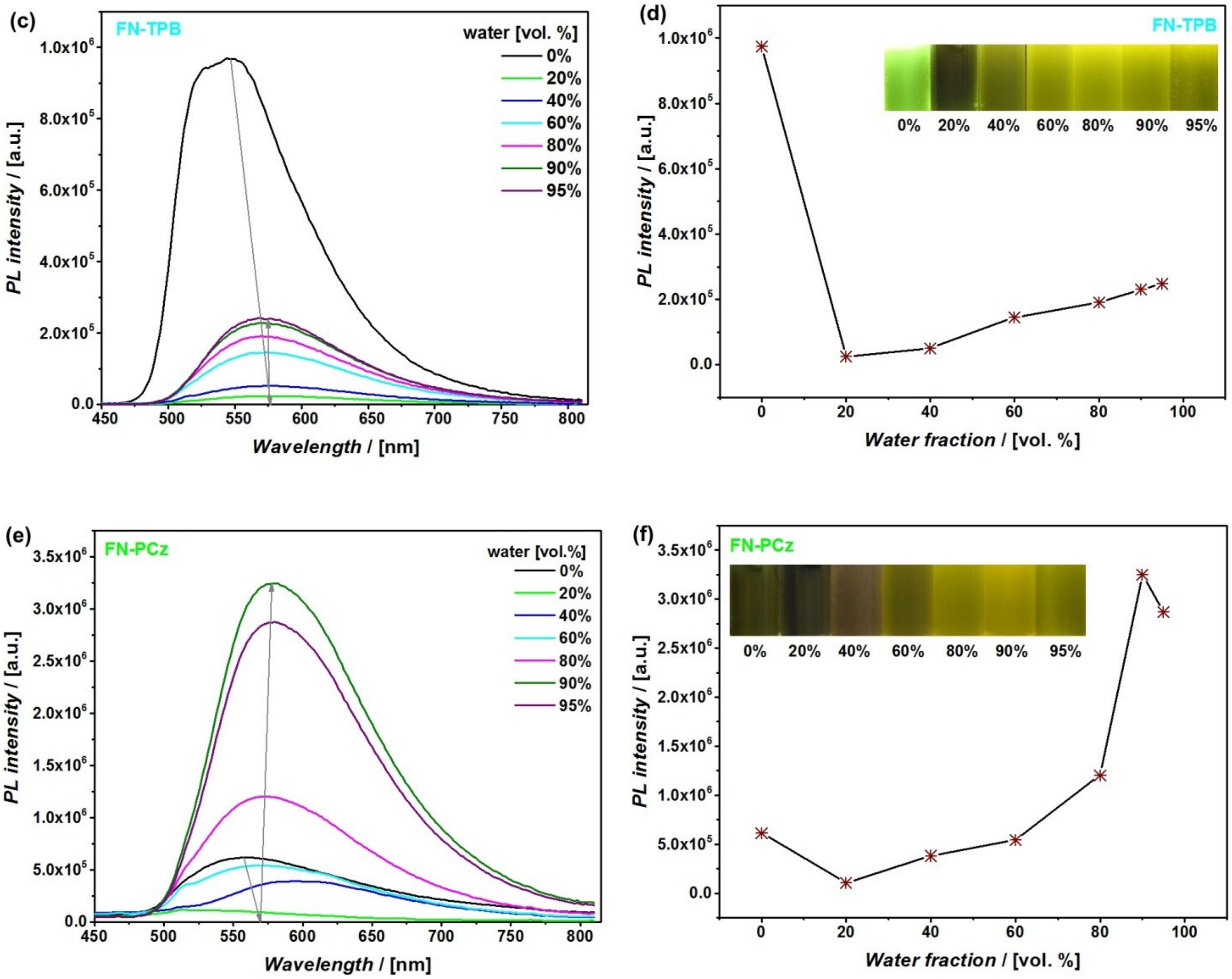

Figure S7. (a, c, e) Photoluminescence spectra of **FN-TPA**, **FN-TPB** and **FN-PCz**, respectively, in different THF/water (v/v) mixtures. (b, d, f) The dependence of photoluminescence intensity of **FN-TPA**, **FN-TPB** and **FN-PCz**, respectively, on the fraction of water.

III. Tables

Table S1. The dipole moments of the monosubstituted fluorenone derivatives, calculated at the BMK/6-31G level of theory in gas phase.

Compound	**Structure**	**Dipole moment / [D]**
FN-TPA$_{half}$	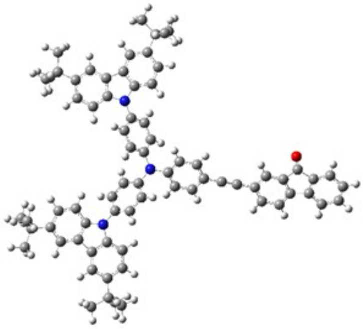	3.44
FN-TPB$_{half}$	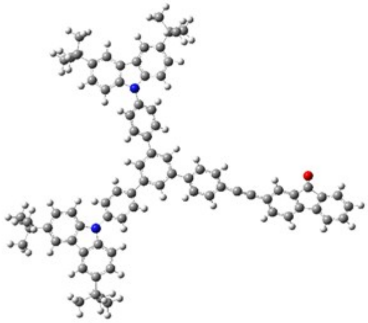	3.69
FN-PCz$_{half}$	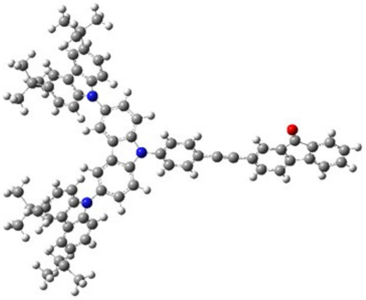	5.98

Table S2. Radiative and non-radiative decay rates constants **FN-TPA**, **FN-TPB** and **FN-PCz.**

Compound	**10^{-5} Hexane solution**		**Zeonex film**	
	Γ^{a} [cm^{-1}]	**$k_{NR}{}^{b}$ [cm^{-1}]**	**Γ^{a} [cm^{1}]**	**$k_{NR}{}^{b}$ [cm^{-1}]**
FN-TPA	0.13	0.04	0.12	0.02
FN-TPB	0.04	0.08	0.07	0.03
FN-PCz	0.10	0.02	0.11	0.01

[a] Calculated by the equation $\Gamma=\eta/\tau$. [b] Calculated by the equation $k_{NR}=(1/\tau)-\Gamma$.

IV. Annexes

Annex I. Charge mobility characteristics

Both hole and electron transport of **FN-TPA**, **FN-TPB** and **FN-PCz** molecules were estimated using a time-of-flight (TOF) method. Electric field dependencies of hole and electron drift mobilities of spin-coated layers of **FN-TPA**, **FN-TPB** and **FN-PCz** are illustrated at Figure S1. The current transients correspond to the dispersive hole and electron transports (Figure S2). Practically, hole and electron mobilities of the compounds are proportional to 10^{-4} cm^2/Vs indicating good ambipolar transport, whereas the values of electron mobility are only slightly higher than those of hole mobility. Mobilities of **FN-TPB** with the 1,3,5-triphenylbenzene fragment reached values of 1.6×10^{-3} cm^2/Vs (for holes) and 2.8×10^{-3} cm^2/Vs (for electrons) at electric field higher than 3.5×10^{5} V/cm. Hole and electron mobilities for **FN-TPB** were found to be higher than those of **FN-TPA** and **FN-PCz**. Considerably higher charge mobility of TPB derivatives was previously observed in our works [3] [18] . The better transport properties of **FN-TPB** as compared to those of the other compounds suggest stronger intermolecular interactions in the solid films [19], in turn being important for the interpretation of the photophysical properties of these compounds.

Annex II. Potential for *J versus H* aggregation

The analysis of the intensity ratio between the 0-0 and 0-1 transitions (Fig. S5), which is very sensitive to the H- or J aggregation [20,21], provides interesting insights on the ground-state aggregation of these compounds in non-polar solvents. Indeed, strong coupling between the excited states on H-aggregated molecules was shown to decrease the 0-0/0-1 intensity ratio, as opposed to strong increase in the case of J-aggregates [20,21]. While both type of aggregations could be expected to occur, cofacial-like aggregations (H-type) seem more sterically hindered due to the peripheral *t*-But bulky groups, whereas J-type (donor-over-bridge) stacking could be easier. The preference for J-type aggregation would also be consistent with the interaction between strong along-chain fluorenone-donor dipole moments. Indeed, our calculations on the monosubstituted ("half-compounds") model analogues of **FN-TPA**, **FN-TPB** and **FN-PCz** result in dipole moments of 3.44-5.98 D at the BMK/6-31G level of theory in gas phase (Table S1). In the frame of this hypothesis, J-type aggregation could then occur for all compounds, however an important effect on the emission spectra (overlap between donor- and bridge localized orbitals) would be expected only in the case of **FN-TPA** due to the important extension of the donor-type orbitals over the bridge (Figure 1 (b), main text). In good agreement with this hypothesis, in the case of **FN-TPB** and **FN-PCz** compounds, comparable 0-0 and 0-1 transition intensities were obtained (Fig. S5), as opposed to the much stronger 0-0 transition intensity as compared to 0-1 observed in the emission spectrum of **FN-TPA** (the 0-1 transition in the case of **FN-TPA** can be detected as a shoulder). This scenario seems to be supported by the PL spectra of solid Zeonex solutions: while only small modifications can be observed in the case of **FN-TPB** and **FN-PCz**, the 0-0/0-1 intensity ratio of **FN-TPA** becomes close to one, which can be safely interpreted as stemming from the reduced presence of intermolecular interactions in solid solutions.

Annex III. Interaction energies in the dimers

The interaction energies (BSSE corrected) in dimers of **FN-PCz** and **FN-di(CC-Ph)** compounds were roughly estimated at the wB97XD/6-31G level in gas phase (Figure S6). To this aim, two dimers with "cofacial" and antiparallel orientation between the average molecular places were constructed in each case. The geometries of each dimer was fully optimized. In the case of antiparallel dimers (corresponding to antiparallel orientation of the molecular dipole moments), interaction energies of 21 kcal/mol and 92.8 kcal/mol were found for **FN-di(CC-Ph)** and **FN-PCz** respectively. These values are overestimated due to the limited basis set employed in these calculations. However, they are expected to remain higher than C=O…..H-C(Ph) H-bonds in these materials independently of the calculation level.

The much larger value corresponding to **FN-PCz** as compared to **FN-di(CC-Ph)** can be easily explained by two effects: (i) quantitative effect: the much larger molecular size of **FN-PCz** results in much larger intermolecular contact (π-π stacking interactions) between the backbones of the two molecules in the dimers. (ii) Several H-bonds can be established by means of the peripheral methyl groups in the case of **FN-PCz**, which are absent in **FN-di(CC-Ph)**[24,25]. These interactions can only reinforce the intermolecular interactions.

Additional test calculations on parallel dimers of **FN-PCz** indicate small relative contribution (< 10%) of the dipole-dipole electrostatic interactions, thus suggesting minor contribution to the intermolecular interactions stemming from the permanent electrostatic multipoles in this type of dimers.

Annex IV. Disaggregation mechanism in FN-TPA, FN-TPB, and FN-PCz

We suggest a two-step disaggregation mechanism for these compounds in THF solvent, which can be imagined according to two different scenarios:

(i) fast breakage of the π-π aggregates (step 1) followed by slow demolition of the H-bonds (step 2), according to the following scheme:

(Strongly bound aggregates) → (H-bonded molecules) → (Free molecules)

(ii) fast relaxation-only of the π-π stacked aggregates (meaning presence of loosely bound aggregates, step 1), followed by slow demolition of the relaxed aggregates and of the H-bonds (step 2), according to the following scheme:

(Strongly bound aggregates) → (Loosely bound aggregates + H-bonded molecules) → (Free molecules)

The presence of the initial and final states is demonstrated experimentally by the presence- and absence of the LEB in the hexane and old THF solutions respectively (Figure 3 (d), main text and our previous study on **FN-PCz** [22]. While both intermediate species satisfy the second requirement (allowing for efficient HBDQ), they differ by the strength of the intermolecular interactions, consisting of only H-bonds in the first scheme, compared to H-bonds and π-π stacking in the second scheme. It is worth remembering that the C=O…..H-C(Ph) H-bonds in these materials are expected to be weaker than the classical H-O…..H-O hydrogen bonds in water. Given that water evaporation takes much less time (several minutes to hours, depending on T and P) than the aging effect in THF solutions of these compounds (1-5 months), it can be safely speculated that the slower process in the aging effect should be the demolition of the relaxed aggregates. This is supported by the important intermolecular interaction energies of several tenths of kcal/mol deduced from our calculations on different dimers of these compounds (Annex II, SI). This result seems consistent with previous studies having reported on the very strong tendency for aggregation in NDI and PDI based compounds. [23] Additionally, several H-bonds can be established by means of the peripheral methyl groups[24,25], which can only reinforce the intermolecular interactions and slow down their dissociation. Finally, the absence of PL quenching in the THF solutions of **FN-TPB** also corroborates the proposed mechanism, given the stronger intermolecular interactions deduced in the case of this compound.

The strong intermolecular interactions in the aggregates, along with the slow diffusion mechanism necessary for the dissociated molecules to escape from the aggregate surface, could thus explain the slow process of total solubilization of these compounds in THF. The important acceleration of the total solubilization obtained by means of sonication [22] seems to support the proposed mechanism, assumedly helping mechanically the destabilization of the π-π stacking interactions- and the faster diffusion of the surficial molecules.

As for the fast observation of the intermediate species (loosely aggregated species) this can be reasonably explained by the electrostatic effect in the polar solvent, resulting in immediate charge (dipole) stabilization and reduction of the intermolecular electrostatic interactions. In the case of **FN-TPB** corresponding to stronger intermolecular interactions, this electrostatic effect is obviously not enough to allow for sufficient intermolecular geometry relaxations and facile reorganization of the C=O…..H-C(Ph) H-bonds in the excited state, thus preventing from efficient HBDQ and PL quenching.

Annex V. Solvent/non-solvent photoluminescence

To further support the ability of the compounds for aggregation, we conducted a solvent/non-solvent photoluminescence test [26,27]. Figure S7 presents the PL spectra of the 10^{-5} M solutions of the compounds in THF/water mixtures with the different volume ratios. With the addition of first water fractions (up to 60% for **FN-TPA** and **FN-PCz**, and 40% for **FN-TPB**), extreme PL quenching was observed for all the compounds. Further addition of water led to the boost of photoluminescence intensities by 45 times for **FN-TPA**, 11 for **FN-TPB** (20 to 95 v.v. % of water) and 26 for **FN-PCz**.

These observations could be explained by two effects: the HBDQ mechanism, and the solubility decrease. We suggest that the extreme PL quenching observed initially is due to the strong HBDQ induced by the strong H-bonding potential of water molecules. In the case of large water %, the solubility factor becomes dominant: since the butterfly-shaped molecules under consideration are insoluble in water, the aggregation is enhanced resulting in emission enhancement [28]. However, unlike it was previously shown for the fluorenone luminogens [28,29], where AIEE phenomenon was proven to originate from the planarization of the molecules and decreasing rotational degrees of freedom, the PL enhancement in the case of our molecules can be interpreted by the transition of the disaggregated but H-bonded species in fresh THF solution (HBDQ) to the emissive aggregated state.

References

(1) de Mello, J. C.; Wittmann, H. F.; Friend, R. H. An Improved Experimental Determination of External Photoluminescence Quantum Efficiency. *Adv. Mater.* **1997**, *9* (3), 230–232.

(2) Miyamoto, E.; Yamaguchi, Y.; Yokoyama, M. Ionization Potential of Organic Pigment Film by Atmospheric Photoelectron Emission Analysis. *Electrophotography* **1989**, *28* (4), 364–370.

(3) Kukhta, N. A.; Volyniuk, D.; Peciulyte, L.; Ostrauskaite, J.; Juska, G.; Grazulevicius, J. V. Structure–property Relationships of Star-Shaped Blue-Emitting Charge-Transporting 1,3,5-Triphenylbenzene Derivatives. *Dye. Pigment.* **2015**, *117*, 122–132.

(4) *Horizons of Quantum Chemistry*; Fukui, K., Pullman, B., Eds.; Springer Netherlands: Dordrecht, 1980.

(5) Frisch, M. J. et al. Gaussian 09, Revision B.02. *Gaussian 09, Revision A.02*. 2009.

(6) Lee, C.; Yang, W.; Parr, R. G. Development of the Colle-Salvetti Correlation-Energy Formula into a Functional of the Electron Density. *Phys. Rev. B* **1988**, *37* (2), 785–789.

(7) Martin, R. L. Natural Transition Orbitals. *J. Chem. Phys.* **2003**, *118* (11), 4775–4777.

(8) Van Regemorter, T.; Guillaume, M.; Sini, G.; Sears, J. S.; Geskin, V.; Brédas, J.-L.; Beljonne, D.; Cornil, J. Density Functional Theory for the Description of Charge-Transfer Processes at TTF/TCNQ Interfaces. *Theor. Chem. Acc.* **2012**, *131* (10), 1273.

(9) Harwood, L. *Experimental Organic Chemistry : Principles and Practice*; Blackwell: Oxford, 1989.

(10) Shi, L.; He, C.; Zhu, D.; He, Q.; Li, Y.; Chen, Y.; Sun, Y.; Fu, Y.; Wen, D.; Cao, H.; Cheng, J. High Performance Aniline Vapor Detection Based on Multi-Branched Fluorescent Triphenylamine-Benzothiadiazole Derivatives: Branch Effect and Aggregation Control of the Sensing Performance. *J. Mater. Chem.* **2012**, *22* (23), 11629.

(11) Lin, T.-C.; Lin, W.-L.; Wang, C.-M.; Fu, C.-W. Synthesis and Characterization of Highly Soluble Two-Photon-Absorbing Chromophores with Multi-Branched and Dendritic Architectures. *European J. Org. Chem.* **2011**, *2011* (5), 912–921.

(12) Weingarten, H. Ullmann Condensation. *J. Org. Chem.* **1964**, *29* (4), 977–978.

(13) Rajwar, D.; Sun, X.; Cho, S. J.; Grimsdale, A. C.; Fichou, D. Synthesis and 2D Self-Assembly at the Liquid-Solid Interface of End-Substituted Star-Shaped Oligophenylenes. *CrystEngComm* **2012**, *14* (16), 5182.

(14) Neugebauer, F. A.; Fischer, H. Tert.-Butyl-Substituierte Carbazole. *Chem. Ber.* **1972**, *105* (8), 2686–2693.

(15) Dewhurst, F.; Shah, P. K. J. Iodination of Fluorenone by N-Iodosuccinimide. *J. Chem. Soc. C Org.* **1969**, No. 11, 1503.

(16) Kim, S. W.; Shim, S. C.; Jung, B.-J.; Shim, H.-K. Synthesis and Properties of New Electroluminescent Polymers Possessing Both Hole and Electron-Transporting Units in the Main Chain. *Polymer (Guildf).* **2002**, *43* (15), 4297–4305.

(17) Cho, D. H.; Lee, J. H.; Kim, B. H. An Improved Synthesis of 1,4-Bis(3,4-Dimethyl-5-Formyl-2-Pyrryl)butadiyne and 1,2-Bis(3,4-Dimethyl-5-Formyl-2-Pyrryl)ethyne. *J. Org. Chem.* **1999**, *64* (21), 8048–8050.

(18) Kukhta, N. A.; Volyniuk, D.; Grazulevicius, J. V.; Juska, G. Effect of the Nature of the Core on the Properties of the Star-Shaped Compounds Containing Bicarbazolyl Moieties. *J. Phys. Chem. C* **2016**, *120* (2), 1208–1217.

(19) Mimaite, V.; Grazulevicius, J. V.; Laurinaviciute, R.; Volyniuk, D.; Jankauskas, V.; Sini, G. Can Hydrogen Bonds Improve the Hole-Mobility in Amorphous Organic Semiconductors? Experimental and Theoretical Insights. *J. Mater. Chem. C* **2015**, *3* (44), 11660–11674.

(20) Spano, F. C. The Spectral Signatures of Frenkel Polarons in H- and J-Aggregates. *Acc. Chem. Res.* **2010**, *43* (3), 429–439.

(21) Spano, F. C.; Silva, C. H- and J-Aggregate Behavior in Polymeric Semiconductors. *Annu. Rev. Phys. Chem.* **2014**, *65*, 477–500.

(22) Kukhta, N. A.; da Silva Filho, D. A.; Volyniuk, D.; Grazulevicius, J. V.; Sini, G. Can Fluorenone-Based Compounds Emit in the Blue Region? Impact of the Conjugation Length and the Ground-State Aggregation. *Chem. Mater.* **2017**, *29* (4), 1695–1707.

(23) Steyrleuthner, R.; Schubert, M.; Howard, I.; Klaumünzer, B.; Schilling, K.; Chen, Z.; Saalfrank, P.; Laquai, F.; Facchetti, A.; Neher, D. Aggregation in a High-Mobility N-Type Low-Bandgap Copolymer with Implications on Semicrystalline Morphology. *J. Am. Chem. Soc.* **2012**, *134* (44), 18303–18317.

(24) Nishio, M. The CH/π Hydrogen Bond in Chemistry. Conformation, Supramolecules, Optical Resolution and Interactions Involving Carbohydrates. *Phys. Chem. Chem. Phys.* **2011**, *13* (31), 13873–13900.

(25) Kodama, Y.; Nishihata, K.; Nishio, M.; Nakagawa, N. Attractive Interaction between Aliphatic and Aromatic Systems. *Tetrahedron Lett.* **1977**, *18* (24), 2105–2108.

(26) An, B.-K.; Kwon, S.-K.; Jung, S.-D.; Park, S. Y. Enhanced Emission and Its Switching in Fluorescent Organic Nanoparticles. *J. Am. Chem. Soc.* **2002**, *124* (48), 14410–14415.

(27) Chen, J.; Xu, B.; Ouyang, X.; Tang, B. Z.; Cao, Y. Aggregation-Induced Emission of Cis , Cis -1,2,3,4-Tetraphenylbutadiene from Restricted Intramolecular Rotation. *J. Phys. Chem. A* **2004**, *108* (37), 7522–7526.

(28) Liu, Y.; Tao, X.; Wang, F.; Dang, X.; Zou, D.; Ren, Y.; Jiang, M. Aggregation-Induced Emissions of Fluorenonearylamine Derivatives: A New Kind of Materials for Nondoped Red Organic Light-Emitting Diodes. *J. Phys. Chem. C* **2008**, *112* (10), 3975–3981.

(29) Liu, Y.; Tao, X.; Wang, F.; Shi, J.; Sun, J.; Yu, W.; Ren, Y.; Zou, D.; Jiang, M. Intermolecular Hydrogen Bonds Induce Highly Emissive Excimers: Enhancement of Solid-State Luminescence. *J. Phys. Chem. C* **2007**, *111* (17), 6544–6549.